ISSN 1063-7761, Journal of Experimental and Theoretical Physics, 2019, Vol. 129, No. 4, pp. 511–520. © Pleiades Publishing, Inc., 2019.
Published in Russian in Zhurnal Eksperimental'noi i Teoreticheskoi Fiziki, 2019, Vol. 156, No. 4, pp. 603–614.

Contribution for the JETP special issue in honor of I. M. Khalatnikov's 100th anniversary

Fragments of the Moon Formation: Geophysical Consequences of the Giant Impact

A. V. Byalko[a],* and M. I. Kuzmin[b],**

[a] *Landau Institute for Theoretical Physics, Russian Academy of Sciences, Chrenogolovka, Moscow oblast, 142432 Russia*
[b] *Vinogradov Institute of Geochemistry, Siberian Branch, Russian Academy of Sciences, Irkutsk, Russia*
**e-mail: alexey@byalko.ru*
***e-mail: mikuzmin@igc.irk.ru*

Received April 2, 2019; revised June 4, 2019; accepted June 6, 2019

Abstract—The most likely scenario for the Moon formation is given by calculations of the Giant Impact (GI) of the ProtoEarth with a protoplanet with a mass close to Mars. During the GI, gases and silicate fragments with a total mass of about 55 to 70% of the mass of the Moon go to infinity, but infinity for the runaway particles is infinity in the terrestrial reference frame. In the Solar System, these fragments go into finite orbits with periods both less and more than a year. The most important feature of their orbits is that they all pass through the region of the Earth's orbit where the GI occurred. A concentrated gas–dust flow was formed there with a fading intensity; it existed for about a million years. Numerically solving the three-body problem yields numerous fragment trajectories. The probabilities of fragments colliding with the Earth and the Moon are estimated as a function of time after the GI. The scenario of fragments falling into the L4 and L5 triangular Lagrange points and the trajectories of their evolution is considered. The most important geophysical consequence of these collisions was the formation of the terrestrial atmosphere and ocean from the concentrated gas–dust flow.

DOI: 10.1134/S1063776119100182

1. INTRODUCTION

The most likely scenario for the formation of the Moon is recognized as a giant impact (GI) of the ProtoEarth with a protoplanet with a mass close to Mars [1]. Based on the age of lunar zircons [2], it occurred about 4.45 ± 0.05 billion years ago, 70–170 million years after the supernova explosion (4568 million years ago), which set the isotopic composition of the Solar System (SS). By the time of the GI, most of the planets had already taken their positions in the SS [3, 4], and the terrestrial planets differentiated gravitationally into iron–nickel cores and silicate mantles, a process facilitated by a powerful but rapidly decaying energy release of the common primary isotopes $^{26}Al \rightarrow {}^{26}Mg$ (0.72) and $^{60}Fe \rightarrow {}^{60}Ni$ (2.6); the half-lives in millions of years are given in parentheses. The depletion of tungsten in the Earth's and Moon's crusts compared with the composition of meteorites is also geological evidence of early differentiation. The reason for this is that the decay $^{182}Hf \rightarrow {}^{182}W$ (8.9 million years) leads to the transition of lithophilic hafnium into siderophilic tungsten, which remains in the iron cores of the emerging planets. This process allows estimating the formation of nuclei of the colliding protoplanets at 30–50 million years after the supernova explosion [5]. The absence of a massive iron core in the Moon also indicates its later formation. As a result of numerous collisions of Moon nuclei with the Earth, a magma trail was formed oin near-Earth orbits, from which the Moon was ultimately formed. Geochemical data on the different concentrations of rare elements in lunar rocks and Earth mantle rocks confirm this observation [4]. We note that lunar zircons have traces of impact genesis in the form of characteristic cracks [2].

The giant impact was repeatedly calculated by the smooth particle hydrodynamics (SPH) method. The results of the best modeling options with 20–30 thousand iron and silicate parts lead to the Moon with the correct mass (1/80 terrestrial) and the silicate composition with 3–4% iron content [6]. As a result, the GI Earth acquires a rapid rotation with a period of about 6 h. The nuclei of the colliding bodies merge into the Earth's core, and the energy released during this process heats it to temperatures around 8000 K. The calculations do not lead to the final formation of the Moon; the Earth was orbited by a particle array, whose relaxation time into a compact body is not precisely defined.

In the collision process, a significant part of the mass goes to infinity. We call these particles the Moon origin fragments (MOFs). Their mass distribution $dN/dm \sim m^{-q}$ ($q = 1.5$–1.8) [1] is close to the distribution of asteroids [7]. The impact of these runaway masses on other SS objects has attracted the attention of astrophysicists with the following concept: the authors of the article [8] tried to find the effect of the MOFs on the asteroid belt in order to explain the late heavy bombardment, traces of which remain on the lunar surface. The size distribution of lunar craters corresponds to the mass distribution of asteroids and MOFs, and the dating of the beginning of the late bombardment, 4.1 billion years ago, is close to the dating of the GI.

Nevertheless, there is no proof of their causal connection. After studying the dispersal of fragments in the SS, we propose a hypothetical scenario that could explain the late bombardment by MOFs falling to the Earth and the Moon.

2. MOF TRAJECTORIES IN THE SOLAR SYSTEM

During the GI, masses of about 56–71% of the Moon's mass or $(5–6) \times 10^{22}$ kg [1, 6] go to infinity. We note that the mass of all modern asteroids is about an order of magnitude less. But infinity for the runaway particles is infinity in the terrestrial reference system; in the SS, almost all MOFs go into final orbits with periods both less and more than a year. A few fastest fragments fly away to the ring of asteroids and into Jupiter's region of attraction. The most important feature of the MOFs is that all of them during the first few thousand periods in the SS fly through the not very extended region of the Earth's orbit where the MOFs had spread during the GI. This statement is true for orbits both in the ecliptic plane and inclined to it (Fig. 1).

After the GI, the Earth continued its motion in an elliptical orbit with an eccentricity close to 0.1, even if both of the colliding protoplanets had circular orbits before the collision. After a year and each subsequent period, the Earth passed very close to the point in the SS where the GI occurred. This situation persisted for several hundred years until the precession of the orbital plane and the displacement of its perihelion diverted the Earth's trajectory to several million kilometers from the GI point.

Those MOFs that acquire a second cosmic velocity after several collisions of large clusters with a rapidly rotating Earth are particularly interesting. This MOF cohort is scattered from the Earth, which is rotating with a surface speed of about 2 km/s, at a speed slightly greater than 11 km/s. The energy spectra of such fragments and of the particles composing the Moon form a continuum. Therefore, this cohort is the largest fraction of the mass of all fragments that flew to infinity in the Earth's reference system. After moving away from the Earth–Moon system, they move in the SS along elliptical trajectories with major semiaxes close to an astronomical unit and with periods close to a year. To calculate the orbits of this MOF cohort, we must solve the three-body problem numerically.

3. ESCAPING IN THE THREE-BODY PROBLEM

A fragment that has flown out in the GI process with a speed substantially greater than the second cosmic speed, after one and hundreds of subsequent periods of revolution, will be at the same SS point with high accuracy. But if its speed is only slightly more than the second cosmic speed, this statement becomes approximate. For further purposes, we must determine the significance of the spread of return points. For this, we investigated the numerical solutions of the three-body problem. In our case, these bodies are the Sun, the Earth–Moon system regarded as a single point, and a fragment with a mass much smaller than the Earth's mass m_E. The parameter of this problem is also the mass ratio of the Earth–Moon system to the Sun's mass m_S.

$$\mu = (m_E + m_M)/m_S = 3.036\times10^{-6}$$

($m_M = 0.012m_E$ is the Moon mass). The smallness of this ratio allows assuming that the center of mass of all bodies coincides with the center of the Sun but does not allow neglecting μ when we study the trajectories of the escaping fragments. In the physical formulation of this problem, there is also uncertainty related to the unknown angle between the impact plane and the ecliptic plane. We use the equations of the three-body restricted problem [9] in a reference frame rotating with the angular velocity of the Earth,

$$\omega = \sqrt{\frac{G(m_E + m_S)}{a^3}} \approx \sqrt{\frac{Gm_S}{a^3}}.$$

Here, G is the gravitational constant, and $a = 1.496 \times 10^{11}$ m is an astronomical unit. The greatest interest for us is the part of the Earth's orbit that is located at a distance of less than 1% of the orbit circumference from the GI point or 3 days in time. In this area, the small eccentricity of the Earth's orbit can be neglected. In the system of astronomical units where $a = 1$ and time is measured in years multiplied by 2π, the trajectory of a body with a negligible mass is then given by the equations

$$\ddot{x} - 2\dot{y} = x - \frac{x}{(x^2 + y^2 + z^2)^{1.5}} - \frac{\mu(x - x_E)}{((x - x_E)^2 + (y - y_E)^2 + (z - z_E)^2)^{1.5}},$$

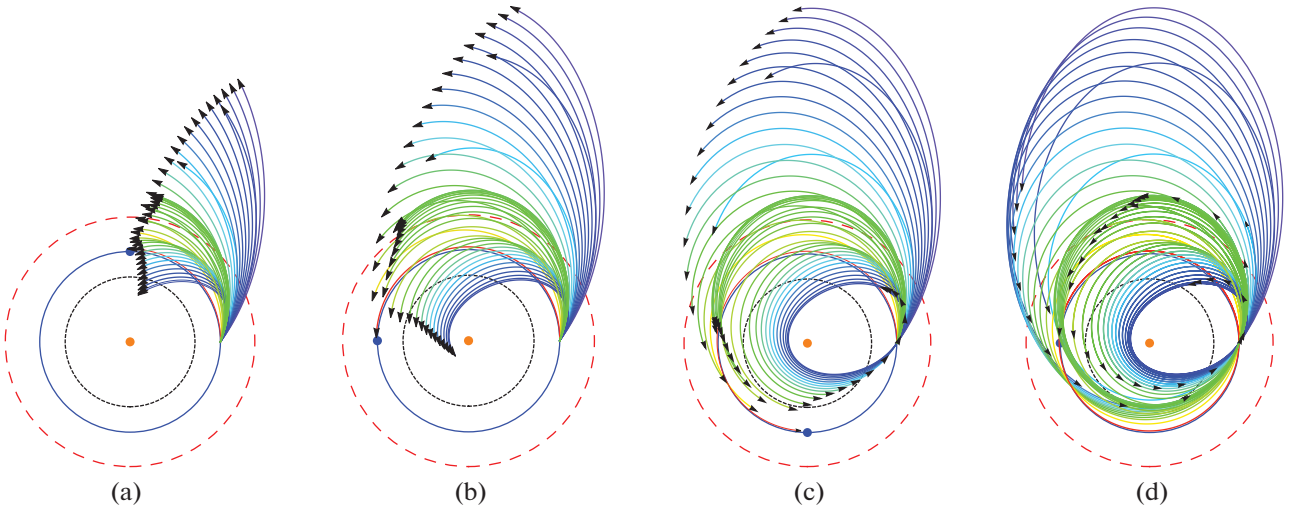

Fig. 1. (Color online) 48 trajectories of the leading cohort of fragments at the beginning of the treatment: their escape rates, depending on the direction, are calculated from the first frames of the GI calculations [6]. The positions of the individual fragments are shown by arrows. All fragments through their period of circulation pass through the GI point with the coordinates (0, 1) with high accuracy. For the scale, the orbits of the Earth (blue circle), Venus (black dashed line), and Mars (red dashed line) are shown. The sun is a yellow disk, and the earth is a blue disk (both not to scale). The position of the fragments after (a) 0.25 year, (b) 0.5 years, (c) 0.75 years, and (d) 1.5 years.

$$\ddot{y} + 2\dot{x} = y - \frac{y}{(x^2 + y^2 + z^2)^{1.5}} - \frac{\mu(y - y_E)}{((x - x_E)^2 + (y - y_E)^2 + (z - z_E)^2)^{1.5}},$$

$$\ddot{z} = -\frac{z}{(x^2 + y^2 + z^2)^{1.5}} - \frac{\mu z}{((x - x_E)^2 + (y - y_E)^2 + (z - z_E)^2)^{1.5}}.$$

We take $x_E = 1$, $y_E = 0$, and $z_E = 0$ as coordinates of the GI point. We then note that the equation for the z coordinate does not play a principal role for our task. The scattering of the slowest, but still escaping, fragments occurred in the equatorial plane of a rapidly rotating Earth, and it generated orbits in the SS with inclination angles i, the magnitudes of which are approximately the same as the inclination of the GI plane to the ecliptic.

As the numerical calculations show, the fragment trajectories passing near the unstable Lagrange points L1 or L2 with the coordinates $(1 \pm (\mu/3)^{1/3}, 0, 0) = (1 \pm 0.001, 0, 0)$ are most critical for determining the orbital motion. Because they are located only 0.01 astronomical units from the GI point, the equation for the vertical z coordinate does not play a significant role for overcoming the potential barrier near L1 or scattering on L2. For fragments flying at an angle i, inclinations to the ecliptic after their entry into orbit around the Sun are projected onto the ecliptic by simple multiplication by $\cos i$. Therefore, we study only numerical solutions of the two-dimensional bounded three-body problem. Its equations are

$$\ddot{x} - 2\dot{y} = x - \frac{x}{(x^2 + y^2)^{1.5}} - \frac{\mu(x - 1)}{((x - 1)^2 + y^2)^{1.5}},$$

$$\ddot{y} + 2\dot{x} = y - \frac{y}{(x^2 + y^2)^{1.5}} - \frac{\mu y}{((x - 1)^2 + y^2)^{1.5}}.$$

The return from the rotating coordinate system $(x(t), y(t))$ to the fixed coordinates $(\xi(t), \eta(t))$ of the SS is performed by the transformation

$$\xi(t) = x(t)\cos t - y(t)\sin t,$$

$$\eta(t) = x(t)\sin t + y(t)\cos t.$$

The initial conditions for the solution are chosen as

$$x(0) = r_0 \cos\vartheta, \quad y(0) = r_0, \quad r_0 = 0.0003,$$

$$\dot{x}(0) = v_0 \cos\vartheta, \quad \dot{y}(0) = v_0 \sin\vartheta.$$

The value of the initial radius r_0 is chosen such that the masses of the forming Moon obviously remain inside it. Numerical solutions essentially depend both on the initial velocity v_0 and on the angles ϑ of departure from the Earth–Moon system. The accuracy of the calculations was controlled by calculating only the first integral of the two-dimensional system of equations, the Jacobi invariant:

$$C_{Jac}(x, y) = x^2 + y^2 + \frac{2}{\sqrt{x^2 + y^2}} + \frac{2\mu}{\sqrt{(x - 1)^2 + y^2}} - (\dot{x}^2 + \dot{y}^2).$$

Its relative variations along all calculated trajectories turned out to be less than 10^{-8}. Various numerical solutions of the three-body problem are shown in

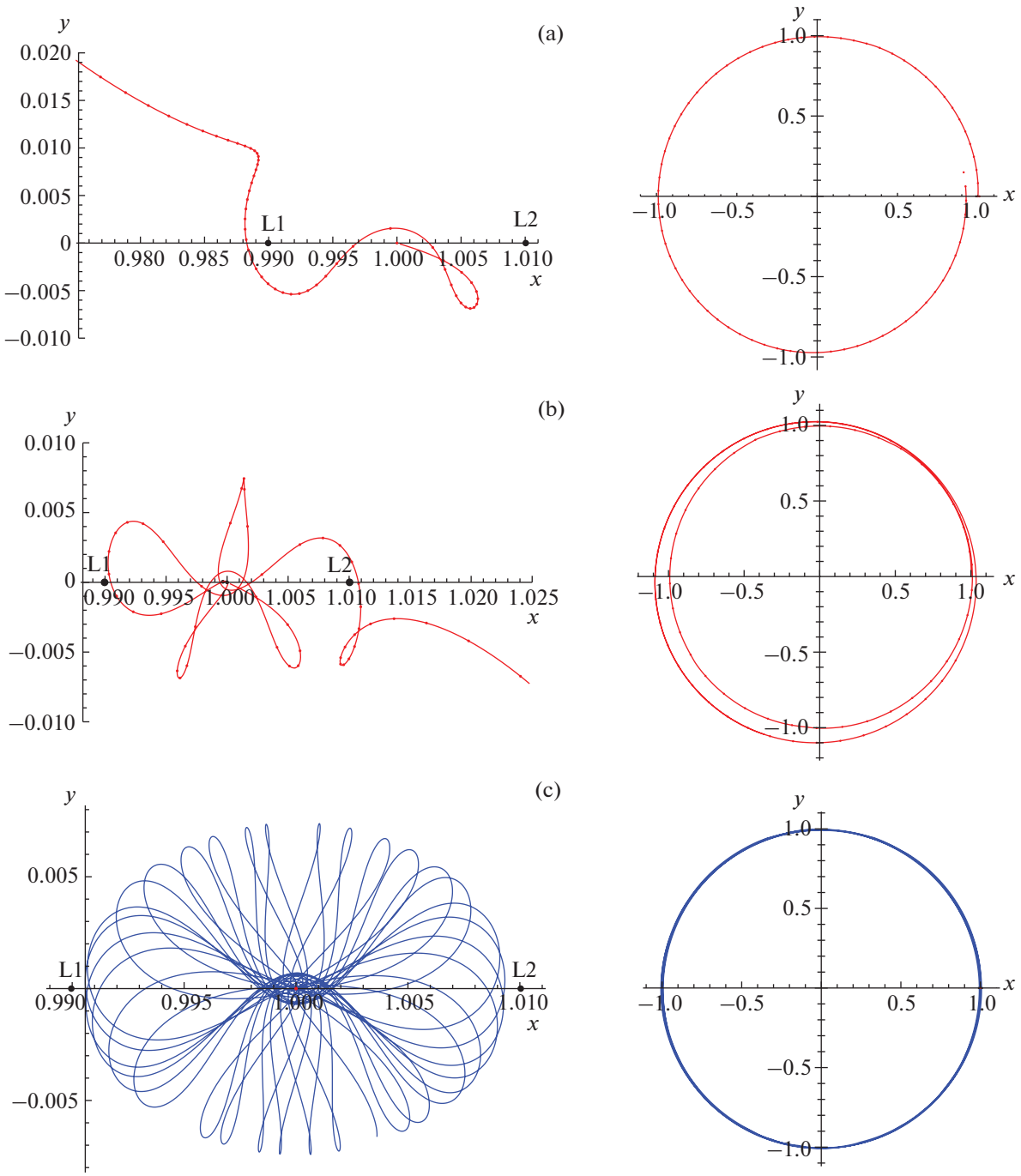

Fig. 2. (Color online) Trajectories of a small body with speeds close to critical: the left and right parts of the figure are respectively given in rotating and fixed reference frames. Dimensionless velocities of the body departure from a distance of 0.0003 AU (7 Earth radii) are (a) 0.39565, (b) 0.3940, and (c) 0.3936. The departure angle in all variants is $45\pi/24$. The exit to the near-solar orbit occurs to the left of the Lagrange point L1 (variant a) or to the right of the Lagrange point L2 (variant b). At a speed lower than the critical one (variant c), the body remains in the Roche cavity near the Earth.

Fig. 2 with a time resolution and in Fig. 3 for different departure angles.

The most important consequence of the obtained solutions can be formulated as follows: the three-body problem has a region of chaotic solutions, where their physical applicability is ensured by the large number of slow MOF cohorts. The calculation results show the following:

1. At speeds lower than critical, a small body remains in an orbit around the Earth, and later after relaxation, the Moon is formed from these bodies.

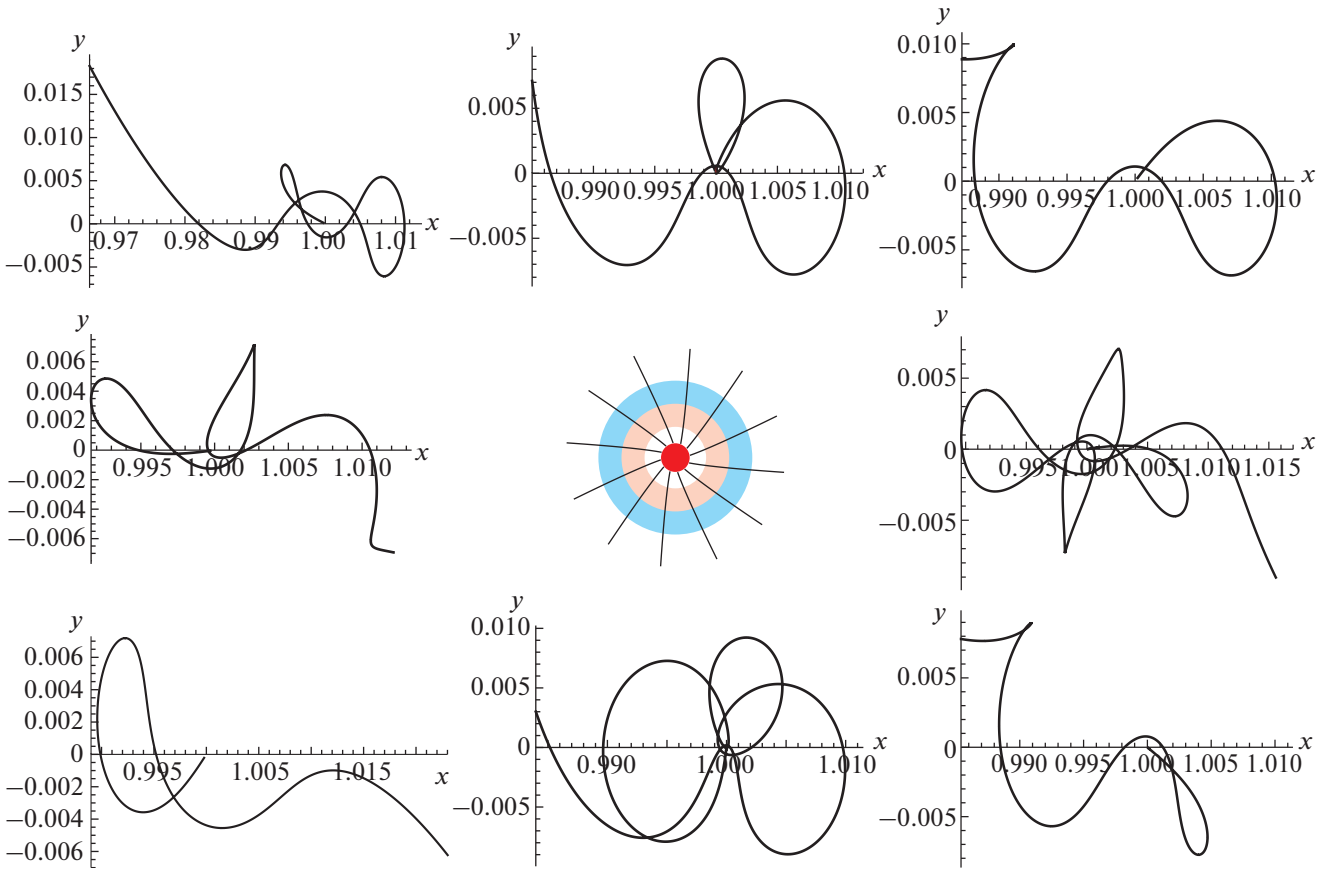

Fig. 3. (Color online) A variety of trajectories of the slowest MOF cohort: the center figure parabolic orbits near the Earth (red circle), crossing the region of the Moon (blue ring) formation. Their initial velocities have a tangential component of about 2 km/s. Along the periphery of the figure, the trajectories of fragments escaping at different angles are represented by numerical solutions of the three-body problem in a rotating reference frame.

2. The critical escape rate depends weakly on the departure angle. At speeds that are only slightly greater than critical, small bodies go around one of the Lagrange points L1 or L2 and go into orbit around the Sun with major semiaxes both smaller and larger than unity. The variance of the chaotic deviations of the major semiaxis from unity is about 0.06.

3. As the speed increases further, the magnitude of the deviation of the return point from the point of departure regularly decreases in absolute value, remaining negative in the case of a flight near the Lagrange point L1 or positive at a flight near L2.

The randomness of solutions and their transition to regular changes is shown in Fig. 4. Chaos is a common property of the three-body problem [10]. In our case, this is one of the sources of the diversity of geophysical consequences of the formation of the Moon.

4. CONCENTRATED GAS–DUST FLOW

In addition to the iron cores and silicate shells, both of the colliding protoplanets probably had their own atmospheres and possibly primary oceans covered with ice, because the Sun's luminosity at the time of the GI was less than the modern luminosity. The influence of ice shells and atmospheres on theoretical calculations of GI is negligible. But when the Earth's surface warms up to $6–8 \times 10^3$ K, all volatile components of the colliding bodies (ice, methane, nitrogen) along with all the crystallization water of thermally decomposed minerals also acquire velocities higher than the Earth–Moon escape velocity. The trajectories of gas molecules coincide with the MOF trajectories. Gases are cooled by adiabatic expansion and are partially condensed on the surface of silicate dust and on massive fragments cooled by thermal radiation. As a result, after several orbital periods, all the material evaporated on impact will fly through the GI region in the form of gas and a multitude of dust bodies covered with dirty ice.

The length of this concentrated gas–dust flow is determined both by the time of formation of the particle belt, from which the Moon is formed, and by the spread of MOF return points to the point of departure, both of which are of the same order. The first of these is the duration of the effective dispersal of the fragments, which is about 2.5 days, as follows from the calcu-

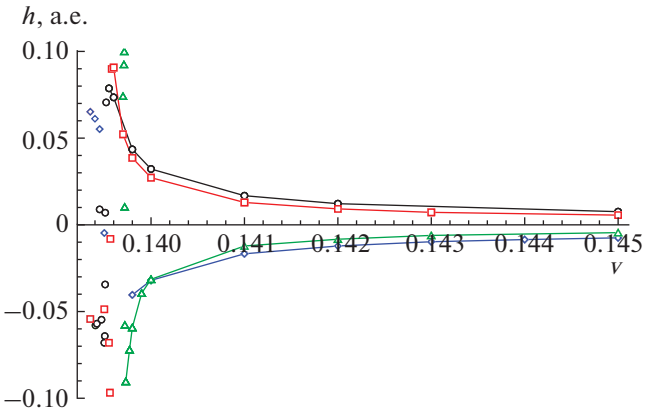

Fig. 4. (Color online) Deviations h of the crossing points from the runaway point depending on the dimensionless speeds v: when the critical velocity is exceeded by 0.3–0.4%, the deviations are chaotic with a standard deviation of 0.059. With a further increase in the runaway velocity deviations, decrease in magnitude without a sign change. Black circles and line for the departure angle $\theta = 0$; red squares and line for $\theta = \pi/4$; green triangles and line for $\theta = \pi$; blue rhombuses and line for $\theta = 5\pi/4$.

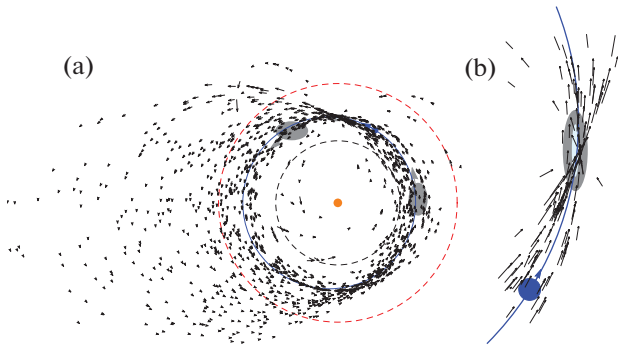

Fig. 5. (Color online) (a) Earth positions (blue circle not to scale) and 1250 MOF particles (black arrows) at 299.8 years after the GI: the Earth's orbit is shown by a blue ellipse with the eccentricity about 0.1, the Venus orbit is shown by a black dashed circle, the averaged Mars orbit is a red dashed circle, and the Sun is a yellow circle (not to scale). Almost all MOF in their movement along elliptical orbits intersect the Earth's orbit in a close vicinity of the GI point. Molecules of nitrogen, water, methane, and other volatile molecules that have flown away from the Earth's surface during the GI process move along the same orbits and form a concentrated gas–dust flow near the GI point. The gas concentration region with a free path of less than 100 km is shown in blue and with a free path of less than 300 km is shown in gray. In these areas, water condensation occurs on the surface of large MOFs and the Earth, and the MOF velocity also aligns with the speed of the Earth. As a result, a noticeable part of the MOFs falls in the regions near the triangular Lagrange points L4 and L5 shown by gray ovals. The stability of the MOFs in these orbits for hundreds of millions of years delays their collisions with the Earth and the Moon. (b) The earth and the region of concentrated gas–dust flow on a large scale.

lations of the GI. The second, the deviation of the slowest orbits from the point of departure after the first revolution around the Sun, has a dispersion of 6×10^{-3} astronomical units.

Consequently, the concentrated flow has a length of $l \sim 6$ million km along the Earth's orbit or about 7×10^{-3} of its circumference. The thickness of the concentrated flow is determined by the angle of inclination of the plane of the GI to the ecliptic, which is unknown but is apparently close to the angle of inclination 20°–30° of the Earth's axis. The thickness of the concentrated flow in both directions perpendicular to the Earth's orbit can be estimated as $(0.1–0.2)l$ or 1 million km in order of magnitude (Fig. 5). We note that the chance of observing similar concentrated flows near other stars is negligible because the lifetime of an intense concentrated flow does not exceed several thousand years.

Taking the mass of the gas in the volume of the concentrated flow equal to 1.5–2 masses of the Earth's ocean, we obtain an estimate of the mean free path of molecules of the order of 30–100 km, which is significantly less than both the longitudinal and transverse dimensions of the flow. The temperature of the gases in the flow cannot be estimated, because their velocity distribution is not Maxwellian. The solar wind also makes a small contribution to the gas component of the concentrated flow. Although the Sun had already emerged from the active T-Tauri stage at the time of the GI, its intensity was several orders of magnitude higher than at present. The role of the solar wind for the gas concentration is insignificant: it is manifested in blowing its light components to the outside.

The impact of small bodies was previously considered in [11], where the deceleration of planets and large bodies by silicate dust, which helps reduce their eccentricities and angles of inclination to the ecliptic, was studied. In addition to these processes, which formed the SS in almost the same plane, small fragments were also considered as a source of late bombardment. Nevertheless, in this work, the stationary stage of the concentrated gas–dust flow and its concentration in that thin region of the SS where fragments scattered after the GI were not considered.

The Earth and the forming Moon fly through the concentrated flow annually with the passage lasting about 3 days. The Earth's surface is rapidly cooled by thermal radiation, and its surface temperature drops below 10^3 K during the year of being outside the concentrated flow. This is enough to keep nitrogen, methane, and water vapor in the Earth's atmosphere. The gases remaining in near-earth orbits after the GI cannot be held on the Moon; they form the first thin atmosphere of the Earth.

The influence of gas and small bodies on the movement of medium and large MOFs and also on the Earth and the Moon is very significant, but it is very difficult to calculate and simulate. Therefore, the following description is qualitative with estimates of characteristic times in order of magnitude. The high-

est concentration of gas and debris in the concentrated flow is provided by the slow MOF cohort; the major semiaxes of their orbits are close to unity, the eccentricities are small, and their speeds do not differ much up or down from the speed of the Earth. The collision cross sections σ with the Earth (and the Moon) are proportional to the square of their radii R, but increase strongly with the approach velocity v_∞:

$$\sigma = \pi R^2 \left(1 + \left(\frac{v_c}{v_\infty}\right)^2\right),$$

where v_c is the escape velocity of the Earth–Moon system, close to 11 km/s. Therefore, a significant part of the bodies of a slow cohort with large axes in the range of 1 ± 0.01 fall to the Earth and the Moon during the first few hundred years after the GI. At the same time, large fragments pierce a thin layer of hardened crust significantly heating the surface.

The gas components of the concentrated flow during this time enrich the Earth's atmosphere, but the condensation of water vapor into the ocean begins only after the Earth's surface cools below 600 K, the critical water temperature, which occurs no earlier than several thousand years after the GI.

The MOF collisions among themselves and also with gas and dust at speeds of several km/s are accompanied by the ionization of gases and the concentration of electric charge on small particles, which accelerate the process of condensation of volatile components on the surface of the fragments. Simultaneously with the condensation of gases in the concentrated flow, many chemical reactions occur with almost all the elements of the periodic table. In particular, the initially reducing nature of the gaseous environment gradually becomes more oxidative, because during shock dissociation of water molecules, oxygen is produced that reacts with metals and gases, and hydrogen is displaced by the solar wind to the periphery of the SS.

The flight of the Earth and all MOFs through a gas–dust flow takes a short time, several days. Intense collisions with dust particles and gas molecules heat a thin layer on the surface of the fragments, and they then cool during the whole period of circulation. Repeated alternation of abrupt heating and relatively long cooling presents the possibility of a qualitative explanation of the appearance of chondras – droplets of molten silicates in the most common type of asteroids, the chondrites.

A few thousand years after the GI, as a result of the precession of the plane of the Earth's orbit and the perihelion displacement, the Earth's trajectory deviates from the GI point, and regular intersections of the concentrated flow stop. The concentrated gas–dust flow in a narrow region of the orbit also disappears because all MOFs as a result of precession change their orbital planes, their perihelion points, and their points of intersection with the earth orbit during this time. Nevertheless, the surviving fragments with high accuracy retain their major axes, eccentricities, and orbital inclinations. As a result, an almost uniform distribution of MOFs relative to the Earth's orbit with small tilt angles is formed.

Collisions of the Earth with MOFs moving in arbitrary orbits can be estimated statistically. The probability w of the Earth and Moon colliding with a fragment whose period is much greater than a year is equal to the ratio of their cross sections πR^2 to the surface through which they sweep in their motion along an orbit of radius a; therefore, $w \sim R/2a$. The value of w is 21×10^{-6} for the Earth and 5.8×10^{-6} for the Moon. This means that the number of MOFs should decrease exponentially quickly with a characteristic time of only 3 million years. It hence follows that already 10 million years after the GI – a negligible time on a geological scale – all MOFs would have disappeared, falling onto our planet and its satellite. By this time, the early heavy bombardment ends. A small part of the MOFs has a chance to reach Mars and Venus, but estimating their share is quite difficult.

5. TEMPERATURE REGIME OF MOFs

Consider the thermal evolution of large silicate MOF with dimensions of 150 ± 50 m, with masses of 10^{10}–10^{11} kg, moving in orbits with large semi-axes in the range of 0.9–1.1 AU. Such MOFs are more likely to come from a slow cohort of debris. Before they were removed from the Earth, they were heated to temperatures of about 10^3 K, therefore, in their initial state, bodies with such dimensions have a spherical shape and a dense dry surface. They cool down slowly enough, which simplifies the qualitative analysis of their thermal conditions. It is determined by one short process with a duration of the order of several days – collisions with gas molecules and small silicate particles at the intersection of the gas-dust flow. Two other relatively long-term effects (with a period of about a year) continue while the MOF moves along the rest of the orbit, it is cooling with heat radiation and heating by insolation.

The thermal characteristics of silicate fragments during the first revolutions around the Sun can be considered close to the density, heat capacity, and thermal conductivity of meteorites [12]:

$$\rho = (3.2\text{–}3.9) \times 10^3 \frac{\text{kg}}{\text{m}^3};$$

$$c_p = 680\text{–}900 \frac{\text{J}}{\text{kg K}}; \quad \kappa = 2.3\text{–}3.9 \frac{\text{W}}{\text{m K}}.$$

The thermal diffusivity of silicate meteorites occurs to be in a rather narrow range

$$\chi = \frac{\kappa}{c_p \rho} (1.03\text{–}1.20) \times 10^{-6} \frac{\text{m}^2}{\text{s}} = 35 \pm 3 \frac{\text{m}^2}{\text{yr}}.$$

During the orbital motion the effect of thermal radiation and insolation penetrates the distance

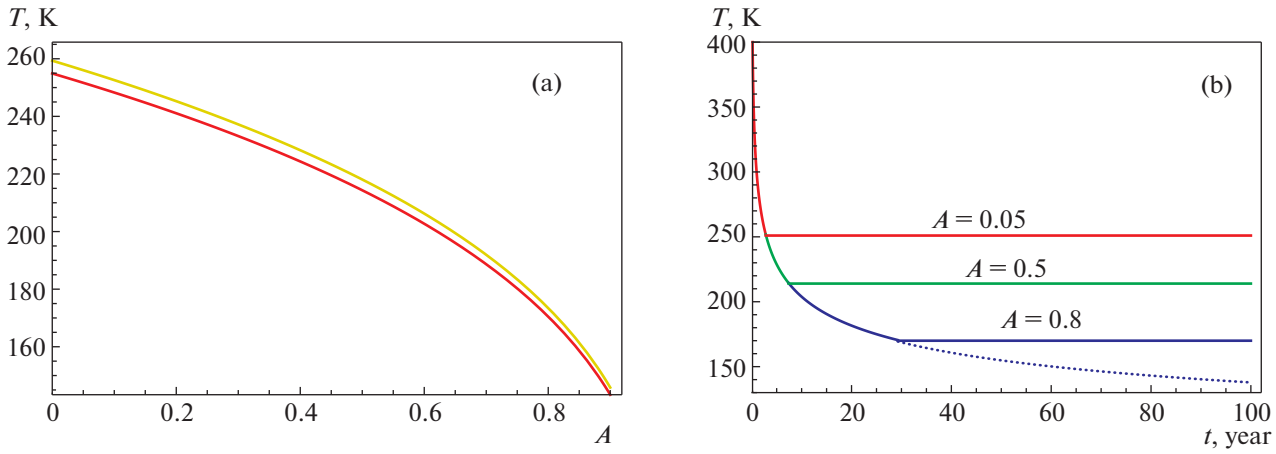

Fig. 6. (Color online) Cooling the MOF spherical surface. (a) Dependence of the surface radiation temperature of on its albedo when illuminated by the faint Sun: the orange curve is for solar luminosity equal to 0.75 of the current one and its temperature equal to 5377 K, the red is for solar luminosity equal to 0.7 of the current one and its temperature equal to 5285 K. (b) General curve and the light-blue filling is the time dependence of the MOF surface temperature in the absence of insolation; the transition to the red level is for the MOF albedo $A = 0.05$; the green transition is for $A = 0.5$; the blue transition is $A = 0.8$.

$D(t) = 2\sqrt{\chi t}$. Over the year, this temperature equalization depth is about 12 m, which is significantly less than the dimensions of the large MOFs we are considering. The luminosity of the Sun during the SS evolutionary period of interest to us was noticeably weaker, it was 70–75% of its current value. The corresponding equivalent temperature of the black radiation of the Sun was $T_{0.7} = 5287$ K or $T_{0.75} = 5377$ K. The radiation temperature of the rotating spherical bodies can be estimated using the well-known formula $T_{\text{rad}} = T_S\sqrt{\frac{R_S}{2a}}(1-A)^{1/4}$, where RS is the modern radius of the Sun and a is the average distance to it (semi-major axis). The graph of T_{rad} versus albedo A is shown in Fig. 6a. In particular, for dark bodies with an albedo of 0.05, the radiation temperature will be close to 250 K.

To estimate the decrease rate of the temperature T of the MOF surface, we will use a simplified radiative cooling formula obtained by integrating the ordinary differential equation

$$\rho c_p \frac{\partial T}{\partial t} = -\frac{\sigma T^4}{2\sqrt{\chi t}},$$

where σ is the Stefan-Boltzmann constant. Since the internal temperature of large MOF during the first revolutions remains significantly higher than the surface temperature, the integration constant can be neglected, as a result

$$T(t) = \left(\frac{9\sigma^2}{\kappa\rho c_p}\frac{1}{t}\right)^{1/6}.$$

The possible error in the numerical coefficient of this formula is overlapped with a double spread of the $\kappa\rho c_p$ product according to [12]. The plot of the decrease in the surface temperature versus time is shown in Fig. 6b together with its transition to radiation temperatures for three albedo values. The graph describes the cooling of large MOFs; smaller fragments have time to cool down over their entire mass and transfer to radiation temperatures earlier than large ones.

This graph does not reflect periodic processes of short heating of the MOF surface when they intersect with the gas and dust flow. Their study is complicated by the uncertainty of the data on the velocities of the flow components, the distribution of small MOF over the masses and the need to simulate collisions and subsequent relaxation. We will attempt to qualitatively describe possible processes in the stream.

The span of the Earth and all MOFs through a gas-dust stream takes a short time, about several days. Intense collisions with dust particles and gas molecules heat GI point (more precisely, the entire flow region) are in the order of magnitude several kilometers per second. The gas stream quickly evaporates ice that could accumulate on the surface of the MOF during a year's orbit. Collision of dust particles at such speeds with the MOF silicate surface leaves craters on it, the size of which depends on the mass of the impactor. The scattering of the silicate material of the crater does not change the situation in the gas-dust flow too much, contributing to the equalization of speeds. The MOF surface at the impact site is locally heated to temperatures that may exceed the melting point of the silicate material. The cooling of the surface at the point of impact due to thermal radiation occurs fairly quickly, but the estimate strongly depends on the intensity of the impact. It is possible that this process forms melt drops characteristic of chondrites.

After repeated intersection of the gas and dust flow area, the state of the surface changes; locally over-

heated parts of the MOF surface are rapidly cooled. For several days of intersection of the flow area, the heating time spreads only to a meter in depth in the order of magnitude, which has little effect on the overall heat balance, determined by the radiation of stored heat and insolation. However, on the cold surface of the MOF, condensation of water vapor occurs, which is entrained by it when it crosses the region of the gas-dust flow, as a result, the albedo of the MOF increases, intensifying their cooling.

6. LATE BOMBARDMENT HYPOTHESES

Dating lunar craters [6, 13] shows that the late heavy bombardment constantly decreased in its intensity. It decayed exponentially with a characteristic time of 150–200 million years for 4.1–3.6 billion years and then with a characteristic time of 500–600 million years from 3.5–1 billion years before our time. For the last billion years, the flow of large asteroids to the Moon (and Earth) has fallen even more with great acceleration [13], almost disappearing in the modern era Currently, the most common explanation for the late heavy bombardment is presented in the works of Morbidelli and his co-authors [3, 14]. It was put forward on the basis of a smart numerical solution on the resonant exchange of places by the orbits of Saturn and Uranus. Note that the choice of initial conditions for these calculations is very conditional. Unfortunately, today there is no theory explaining the distribution of the torque in the SS, where the whole rotational moment remained in the giant planets. The initial conditions of this task have been chosen artificially to provide the planets exchange, but in principle such a scenario is possible.

However, the exchange of orbits, which shook the SS, occurred only about 10 million years from the beginning of the calculations. The authors do not indicate its absolute dates, but it is natural to assume that the physical zero of reference should be at a moment close to the formation of SS. In this case, the dating of the late bombardment is so far behind the start of the calculations that the hypothesis of the Morbidelli group [14] raises reasonable doubts.

We propose a different hypothesis for the accelerated decay of late bombardment; this scenario has not been previously considered. It consists in the fact that the bodies that turned out to be near Lagrange points L4 and L5 (they are located at angles of $\pm 60^\circ$ relative to the Earth in its orbit) move for a long time along stable paths. The process of capturing fragments in L4 or L5 seems quite natural due to the existence of a gas-dust flow in the vicinity of the GI point. The triangular points of Lagrange, like the Earth, passed annually through a gas-dust jet stream. At such moments, with a significant probability, two MOF could collide, one of which is slightly slower than the Earth's orbital speed, and the other more. As a result of the loss of speed during a collision, one or several bodies moving along stable orbits in the region of triangular Lagrange points occurred. The dust from several such collisions slowed down the speeds of larger bodies, increasing the stability of their orbits near triangular points.

Estimation of the probability of a possible exit of a body from a stable region between L4 and L5 is quite complicated. There is no rigorous proof of the role of the triangular Lagrange points to explain the late heavy bombardment, this hypothesis certainly needs a more detailed confirmation by numerical three-dimensional calculations. Currently, only one 300-meter asteroid 2010TK is detected near the Lagrange point L4. It was discovered by the WISE infrared space telescope in 2010. Its period is 1.00346, the eccentricity is 0.19084, and the inclination of the orbit is 20.88°.

7. GEOLOGICAL CONSEQUENCES

The most important consequence of the proposed scenario is a radical change in the generally accepted scenario of the origin of the terrestrial ocean. The concept adopted in geology is that it was formed by the release of juvenile waters in the process of gravitational differentiation, but the concept of the Moon formation during the GI completely eliminates this generally accepted view. The surface of the Earth, which melted at high temperatures immediately after the GI, was devoid of even traces of moisture. The first entry of gases into the atmosphere (including water vapor) occurs during the first hundreds years after the GI, when the Earth repeatedly passed through a concentrated gas–dust flow. These collisions supplied the planet with nitrogen, methane, ammonia, and water, creating a primary reducing atmosphere and ocean. During 10 million years after the GI, the Earth captured nearly all gases except hydrogen and helium and also all MOFs except those fragments that were captured near the triangular Lagrange points.

The stages of the decrease in the total mass of the MOFs and also the formation stages of the Earth's atmosphere and ocean are presented qualitatively in Fig. 7.

We note that the transition to an oxidizing environment on Earth may have begun at about the same time. On Earth, there are no rocks of the crust that were destroyed by early bombardment; they fell into the mantle and melted. Only refractory zircons, which were formed from small amounts of acid (granite) melt, have been found. The dating of these zircons belongs to the interval from 4.4 to 4.1 billion years ago. The terrestrial zircons have a cerium anomaly in the distribution of rare-earth elements compared with chondrites [5] and lunar zircons. This fact indicates that by this time an aqueous and partially oxidizing environment had already formed on Earth, while only a reducing environment was observed in all lunar zircons.

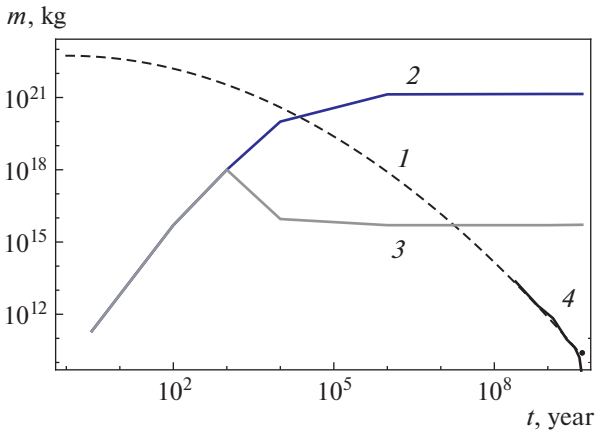

Fig. 7. (Color online) Changes in the total mass of the MOF (black dashed curve) and also the masses of the Earth's atmosphere (blue broken line) and ocean (gray broken line) after the GI: the MOF mass decreases as a result of collisions with the Earth and the Moon. Earlier than 10^3 years, the temperature of the earth's surface prevents the condensation of water, and the atmosphere comprises nitrogen, methane, and ice MOF in the form of water vapor. The condensation of the ocean then begins and increases to the present mass in 10^4–10^5 years after the GI. After 10^6 years, all MOFs in ordinary SS orbits disappear in collisions with the Earth and the Moon, and fragments remain only in the vicinity of the Lagrange triangular points. The stage of late bombardment begins (2×10^8–10^9 years after the GI or 1.5–3.5 billion years ago). The dynamics of mass loss during this period is shown according to [8, 13] obtained by dating lunar craters ages (black curve), but the end of the dotted curve (bold dot) corresponds to a large asteroid 2010TK from the vicinity of L4 with a mass of 3×10^{10} kg.

Other significant geological consequences of the GI are volatile metallic compounds that left Earth together with silicates during the collision of protoplanets and then returned to it and the Moon during both the early and the late bombardment [13, 15]. Anomalies of such elements as indium, cadmium, zinc [16, 17], and potassium [18] have been found. The anomaly of different ratios of two neon isotopes in the Earth's atmosphere, the solar wind, and chondrites [19] is not explained in the framework of the studied processes that occurred with fragments of the Moon formation.

8. SUMMARY

Quantitative solutions of the restricted three-body problem have been obtained, showing the reality of the formation of a concentrated gas–dust flow in the region of the SS where the GI occurred. Other numerical solutions show the stability not only of the triangular Lagrange points themselves but also of the belt connecting them. The proposed concept of evolution of the fragments of the Moon formation leads to a number of geophysical consequences, among which the most important are the qualitative description of the transition from early to late bombardment and also the formation of the Earth's atmosphere and ocean.

All calculations and illustrations of this paper were performed using the Wolfram Mathematica Version 12.0 software.

REFERENCES

1. R. M. Canup and E. Asphaug, Nature (London, U.K.) **412**, 208 (2001).
2. T. M. Harrison. A. K. Schmitt, M. T. McCulloch, et al., Earth Planet. Sci. Lett. **268**, 476 (2008).
3. K. Tsiganis, R. Gomes, A. Morbidelli, et al., Nature (London, U.K.) **435**, 459 (2005).
4. K. C. Condie, *Earth as an Evolving Planetary System* (Elsevier, Amsterdam, 2011).
5. M. I. Kuz'min, V. V. Yarmolyuk, and A. B. Kotov, Litosfera **18**, 653 (2018).
6. R. M. Canup, Icarus **168**, 433 (2004).
7. P. Brown, R. E. Spalding, D. O. ReVelle, et al., Nature (London, U.K.) **420**, 294 (2002).
8. W. F. Bottke, D. Vokrouhlicky, D. Minton, et al., Nature (London, U.K.) **485**, 78 (2012).
9. A. E. Roy, *Orbital Motion*, 4th ed. (IOP Publ., Bristol, 2005).
10. S. Liao, Commun. Nonlin. Sci. Numer. Simul. **19**, 601 (2014).
11. H. E. Schlichting, P. H. Warren, and Q.-Z. Yin, Astrophys. J. **752**, 8 (2012).
12. E. N. Slyuta, Solar Syst. Res. **51**, 64 (2017).
13. S. Mazrouei, R. R. Ghent, W. F. Bottke, et al., Science (Washington, DC, U. S.) **363**, 253 (2019).
14. R. Gomes, H. F. Levinson, K. Tsiganis, and A. Morbidelli, Nature (London, U.K.) **435**, 466 (2005).
15. C. A. Norris and B. J. Wood, Nature (London, U.K.) **549**, 507 (2017).
16. Z. C. Wang, V. Laurenz, S. Petitgirard, et al., Earth Planet. Sci. Lett. **435**, 136 (2016).
17. R. C. Paniello, J. M. D. Day, and F. Moynier, Nature (London, U.K.) **376**, 290 (2012).
18. K. Wang and S. Jacobsen, Nature (London, U.K.) **538**, 487 (2016).
19. C. D. Williams and S. Mukhopadhyay, Nature (London, U.K.) **565**, 78 (2019).